

Photodegradation of Cationic Dyes in Aqueous Solutions by BiOI/SrHA Nanoparticles

Mohammed K. Kzar¹

¹ Department of Chemistry, College of Science, University of Basrah
Basrah, Iraq
Corresponding author's E-mail mohammedkadhikzar@utq.edu.iq

Zaki N. Kadhim²

² Department of Chemistry, College of Science, University of Basrah
Basrah, Iraq
Second Author's E-mail Zaki.kadhim@uebasreh.edu.iq

Ali H. Al-Mowali³

³ Department of Chemistry, College of Science, University of Basrah
Basrah, Iraq
Third Author's E-mail ali-almoaali1946@yahoo.com

ABSTRACT

In this research, we discuss the removal of basic fuchsin (BF), and crystal violet (CV) dyes by strontium hydroxyapatite supported BiOI. A modified hydrolysis model, one can synthesise BiOI/SrHA. BiOI/SrHA was characterized using Fourier transform-infrared spectroscopy (FTIR), UV-visible (UV-vis) analysis, X-ray diffraction (XRD), energy diffraction X-ray (EDX), and scanning electron microscopy (SEM). SEM outcome confirmed the dispersion of BiOI onto strontium hydroxyapatite. The shape of the BiOI catalytic samples overlapped with each other to form 3D hierarchical flower-like structures. The UV-visible was used as a radiation source during photocatalysis. BiOI/SrHA had an effect on malachite green dye degradation. The oxidative removal occurred through hydroxyl radical formation. UV-visible (UV-vis) BiOI/SrHA showed perfect photocatalytic property for the decay of Basic Fuchsin (BF) and Crystal Violet (CV) from an aqueous solution. According to kinetics analysis, the dye degradation rates could be in a pseudo-first-order model.

Keywords:

bismuth oxyiodide (BiOI), strontium hydroxyapatite (SrHA), cationic dyes, photocatalytic, XRD, EDX, and SEM

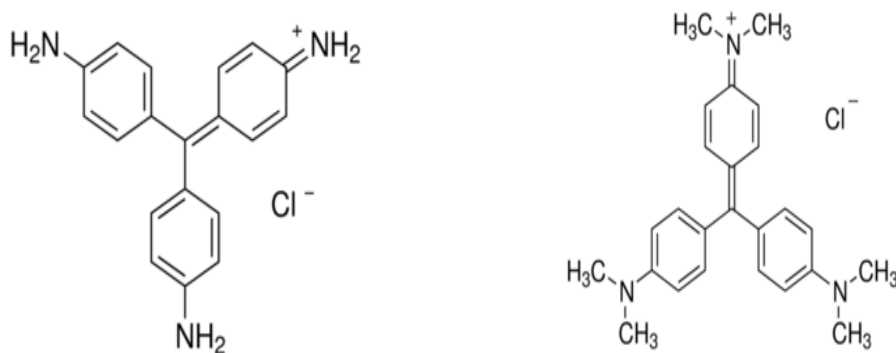
1. Introduction

Pollutants can be elements, molecules, or particles that have a great impact on living organisms and cause problem to the environment⁽¹⁾. Plants and trees cannot grow in the absence of clean water. That is, there is no source of food, and this, in turn, can affect the economic conditions of humans, and here we must admit that people are the main source of environmental pollution⁽²⁾. One of the most

important water pollutants is included insecticides and herbicides, nutrition processing waste, pollutants from cattle operations, volatile organic compounds, heavy metals, chemical waste, and others^(3,4). Many of these factors that are important, especially for the production and distribution of healthy drinking water, Furthermore, several water factors are of fateful importance to the optimal process of Advanced Oxidation Processes (AOPs), such as the alkalinity, the pH, the

transmittance, or absorbance, and temperature of the water, play a great role in photochemical water purification processes. Recently, the world has paid a lot of attention to the photocatalytic process. In, this field researchers and scientists have conducted many types of experimental research. Heterogeneous photocatalysis is a promising new alternative method for the removal of organic pollutants from water. The photocatalytic mechanism is based on the advanced oxidation process(AOP), which has shown a high ability to decompose, mineralize harmful organic and inorganic compounds in the environment. One of the most important compounds that were used in the photocatalytic process is TiO_2 and ZnO , The importance of these two compounds is there non-toxicity and for their strong oxidizing power. The incorporation of bismuth into a given material yields an additional filled Bi 6s state, which appears to be more than 0 2p. The transition to the s/d states of a transition metal from Bi 6s (or hybrid Bi 6s-O 2p states) becomes possible, which decreases the bandgap. Compounds of the bismuth oxyhalide (BiOX) group exhibit some semiconducting and optical properties. In 1935, the scientist Bannister discovered the BiOX crystal structure and found that it possessed layers linked by covalent bonds of the three elements that it made up $[\text{X-Bi-O-Bi-X}]$, and $\text{X} = \text{halogens Cl, Br, I}$ respectively^(5,6). The geometric structure of BiOI/SrHA is tetragonal, so an electric field can be generated work that activates photocatalytic thus preventing recombination between electron and Holes formation⁽⁷⁾. Zhang et al. (2006) investigated the photocatalytic properties of bismuth oxyiodide (BiOI) as the first BiOX compound⁽⁸⁾. In recent years, there

have been many medical, domestic, and industrial pollution problems. So As a result, efforts have been made to address this serious issue through practical research⁽⁹⁾. In this field, nanoparticles have been used extensively to reduce this dangerous phenomenon⁽¹⁰⁾. Many nanomaterials have been used, including bismuth oxyhalide BiOX , and these compounds are distinguished by the fact that they have unusual properties that make them distinguished compounds in this field. The formed Bi nanoparticles on the BiOI surface accelerate the transfer of photo-induced electrons from BiOI to Bi, and the surface oxygen vacancies on the BiOI photocatalyst result in its bandgap narrowing to the visible light range⁽¹¹⁾. Many experiments have been carried out in the process of replacing the element strontium (Sr^{+2}) to replace the element calcium (Ca^{+2}) in the compound hydroxyapatite, particularly in biological experiments, specifically in bones, where experiments have proven that the element strontium (Sr^{+2}) is non-toxic and stable when bound to hydroxyapatite⁽¹²⁻¹⁶⁾. BiOI displays a small bandgap (~ 1.7 eV) and is an active visible-light photocatalyst for the photodegradation of different pollutants⁽¹⁷⁻¹⁹⁾. Li et.al offers BiOI with 3D hierarchical structures applied in the degradation of methyl orange (MO) and phenol with the effective photocatalytic action⁽²⁰⁾. Zan et.al elucidate that the photodegradation efficiency of cationic Rhodamine B (RhB) with BiOI was increased highly due to its distinctive structure containing single-crystal nanosheets with high symmetry⁽²¹⁾. The structure of the two dyes examined is depicted in Figure1.



Basic Fuchsin (BF)

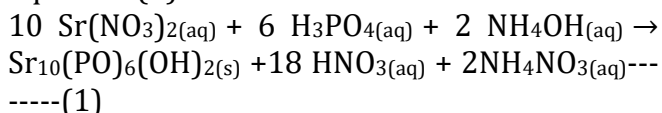
Crystal Violet (CV)

Figure 1: The chemical structure of dyes

2. Experimental

2.1. Preparation of SrHA

The Synthesis of SrHA was performed the method previously described ^(22,23). A solution of H₃PO₄ 0.3 mol. L⁻¹ was vigorously mixed with a solution of Sr(NO₃)₂ 0.5 mol. L⁻¹ (Merck, 99.67%) (molar ratio Sr/P = 1.67. By adding NH₄OH (Merck, 30%), the pH of the solution was adjusted to 9.0. A white precipitate was formed, and the suspension was stirred for 2 h. Thereafter, the precipitate was washed with distilled water and vacuum filtered. The preparation reaction occurs according to equation (1).



2.2. Preparation of BiOCl/SrHA

BiOCl/SrHA nanoparticles were synthesized by a modification hydrolysis method using bismuth oxide, Hl, and SrHA as precursors. The Bi₂O₃ (1.5g) was dissolved in excessive concentrated hydrochloric acid (10 mol/L, 10 mL) to obtain a transparent BiO₃-Hl aqueous solution. To this solution, 1.2 g of SrHA was added with simultaneous stirring. The obtained mixture was sonicated for 15 min. The pH of the solution was adjusted between 2 and 3 using ammonia. The mixture was heated at 90 °C for half an hour to obtain white precipitates. The precipitates were washed several times

with water and ethanol and then dried at 75 °C for 10 h. The acquired product is calcined in an electric furnace for 3 h at 550 °C. to obtain BiOCl/SrHA nanoparticles.

3. Photocatalytic Dyes Degredation And Reactor

A photoreactor (as seen in Figure 2) experiment was carried out in a mode photoreactor. It was irradiated with UV light using ($\lambda=254\text{nm}$, 30V). The photocatalytic dye's degeneration tests were operated by mixing different amounts of BiOCl/SrHA nanoparticles in a photoreactor with a capacity of 1000 mL of each dye solution (15, and 20 mg/L, respectively) at 25°C. At predictable time intervals, the solution patterns were removed from the reaction medium. With the use of a UV-vis spectrophotometer (Perkin-Elmer Lambda 25), we separate BiOCl/SrHA from the solution and observe the change in the catalyst adsorption process for these dyes at maximum wavelengths 545 and 591 nm for Basic Fuchsin and Crystal Violet, correspondingly. The concentration of BiOCl/SrHA nanoparticles has an effect on the degeneration of photocatalytic dyes by contacting 1000 mL of dye solution (15 and 20 mg/L for Basic Fuchsin and Crystal Violet, respectively) at room temperature of 25°C for 5 h. Various amounts of BiOCl/SrHA nanoparticles were used. Initial dye concentration was calculated to see how it

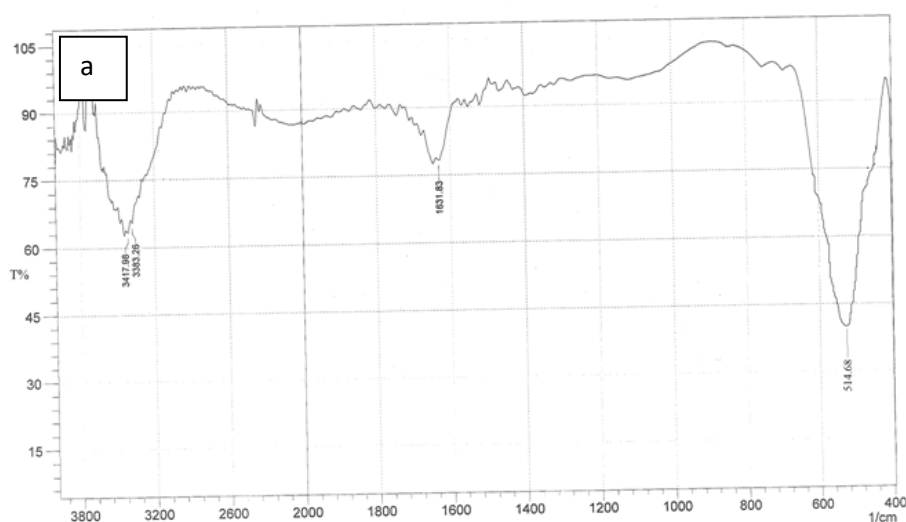
affects photocatalytic dye degradation. The BiOI/SrHA nanoparticles (0.05 g Basic Fuchsin, and 0.05 g for Crystal Violet) were added to 1000 mL of different dye concentrations (15, 30, 45, and 60 mg/l) of Basic Fuchsin (BF) and (20, 40, 60, and 80 mg/l) of Crystal Violet (CV).

4. Results And Discussion

4.1. Characterization of specimens

Figure 3 shows the FT-IR spectra of BiOI/SrHA, the range of (3417.98 – 3346.76) cm^{-1} may refer to the stretching vibrations of –OH that existed in the adsorbed water molecule. As well the distinctive peaks at range (1615.41) cm^{-1} are referring to the O-H bending vibrations. for pure BiOI, 442.73 cm^{-1} corresponds to valence symmetrical (A_{2u}-type) vibrations of the Bi-O bond, a reference that the compounds of BiOI are obtained. The broadband at 3417.98 cm^{-1} is refer to O–H vibration of H₂O absorbed in the specimen. 1404.71 cm^{-1} peak is refer to the carbon-related pollution and a small amount of (CO₃)²⁻ caused by the CO₂ in an aqueous solution or air during the synthesis. 1615.41 cm^{-1} peak is refer to carbon-related pollution. The bands at 1018.19 is a marker of asymmetric stretching. The two groups of bands in the low wavenumber ranging from 605.22-510.04 cm^{-1} are attributed to the

bending vibrations of O–P–O in (PO₄)³⁻ groups. confirmed the formation of BiOI/SrHA. Figure 4 note sample BiOI/SrHA overlapped with each other. The morphology of BiOI/SrHAp diagnosed by scanning electron microscopy (SEM) are fixed in SEM visual data shows a quite different morphology. notable, the surface structure of BiOI/SrHA changes to marked rise with some holes which look like bunches of grapes that were not present before being installed when modified, This explains the presence of a large surface area, which increased the adsorption process of the dyes Basic Fuchsin, and Crystal Violet, widely used dyes, were chosen as the test pollutant to evaluate the photocatalytic activity of synthesized BiOI/SrHA. The phase structures of the as-synthesis BiOI/SrHA specimens were examined by XRD. As displayed in Figure 5 peaks from BiOI/SrHA sample appear at 13.1, 23, 27.3, 31.7, 32.8, 35.25, 39.95, 40.95, 42.95, 46.25, 49.55, and 58.53, 2 θ values with corresponding hkl values as 002, 012, 110, 013, 004, 020, 005, 114, 122, 016, 025, and 017, respectively, as per JCPDS card No. 73-2062.[20].describe the EDX pattern of BiOI and BiOI/SrHA. in Figure 6, The presence of the components O, P, I, Sr, and Bi in BiOI/SrHA verified its formation.



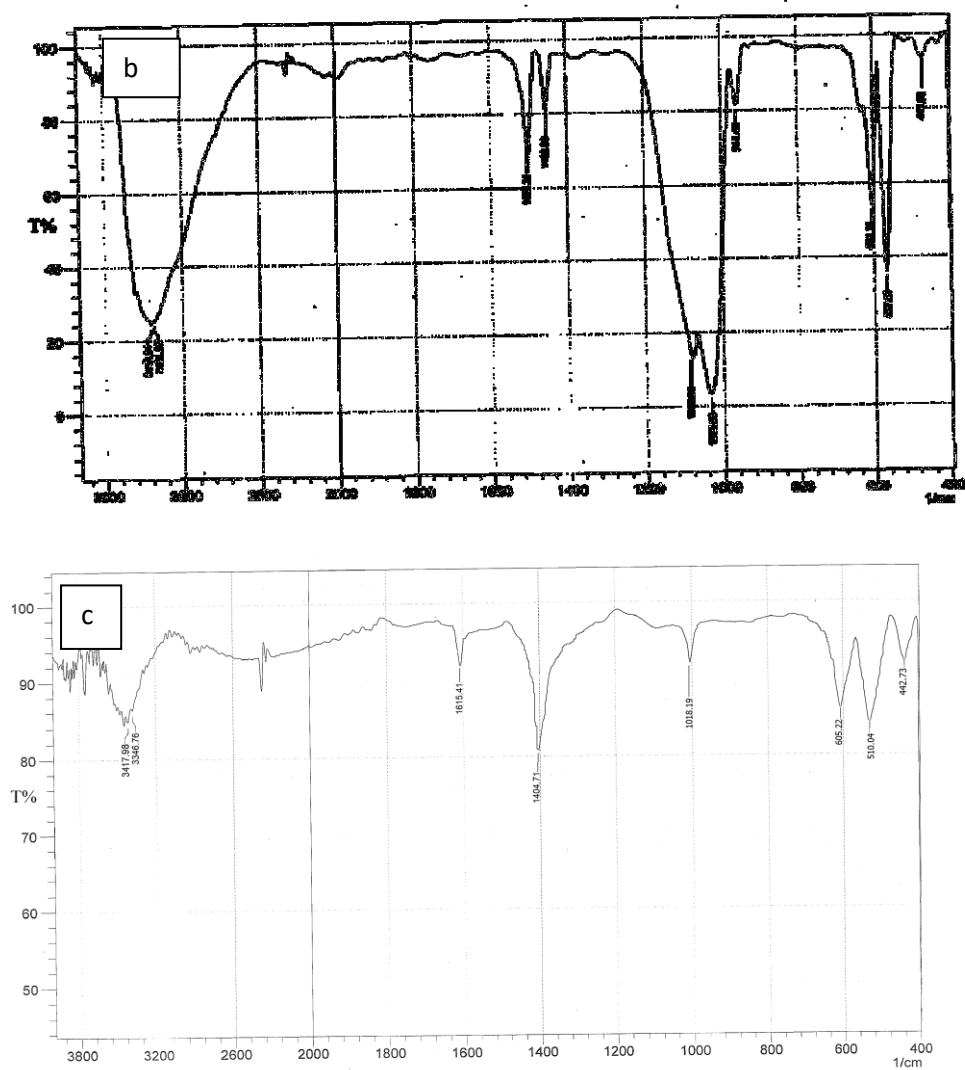


Figure 2: FTIR patterns of (a) BiOI, (b) SrHA, and (c) BiOI/SrHA

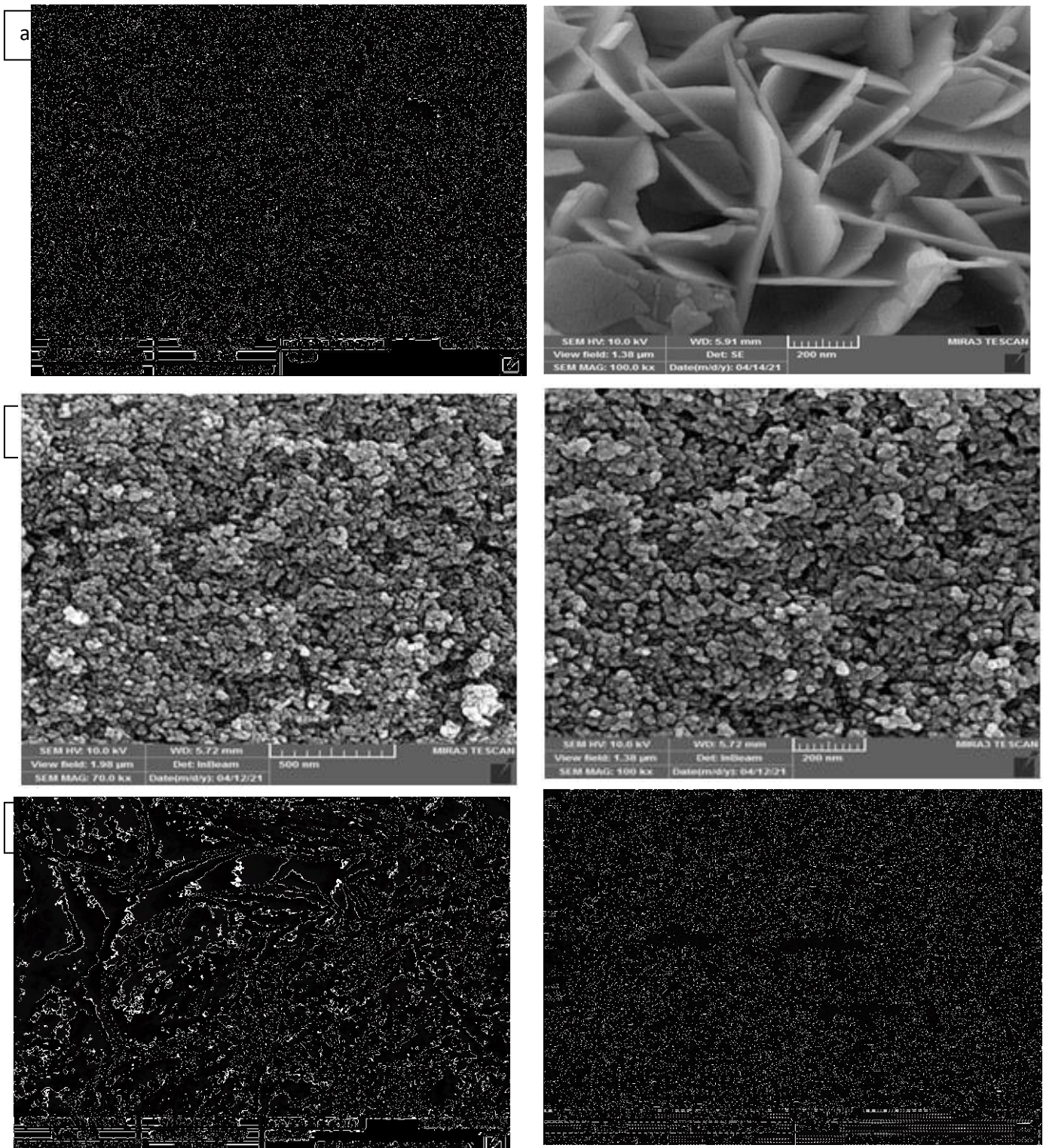


Figure 3: SEM of BiOI (a), SrHA (b) and BiOI/SrHA (c)

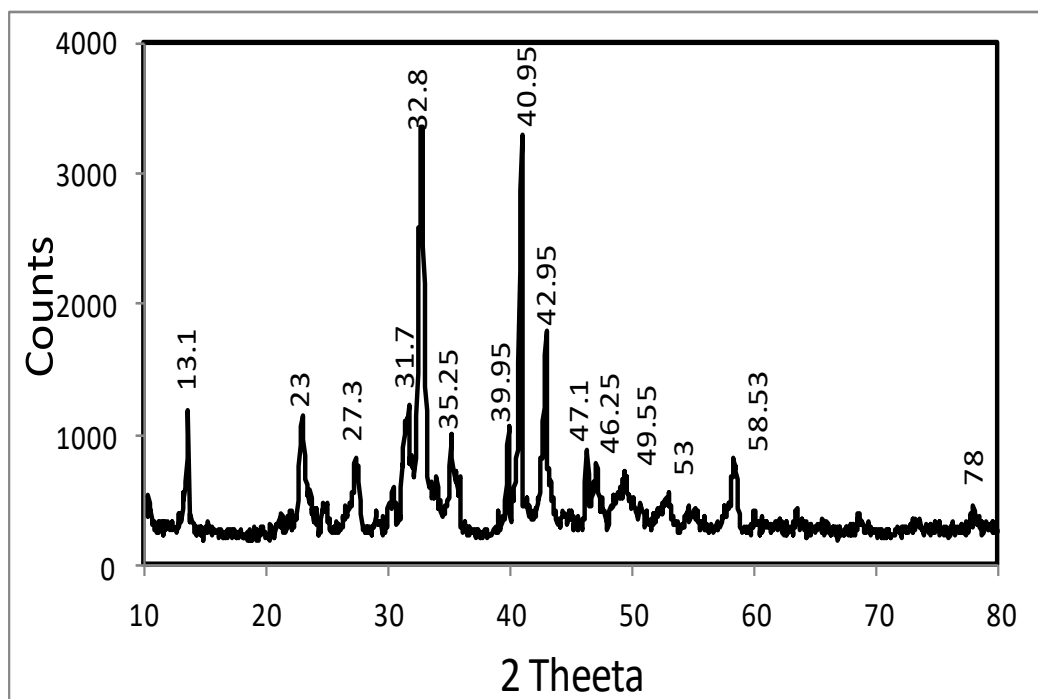


Figure 4: XRD patterns of BiOI/SrHA

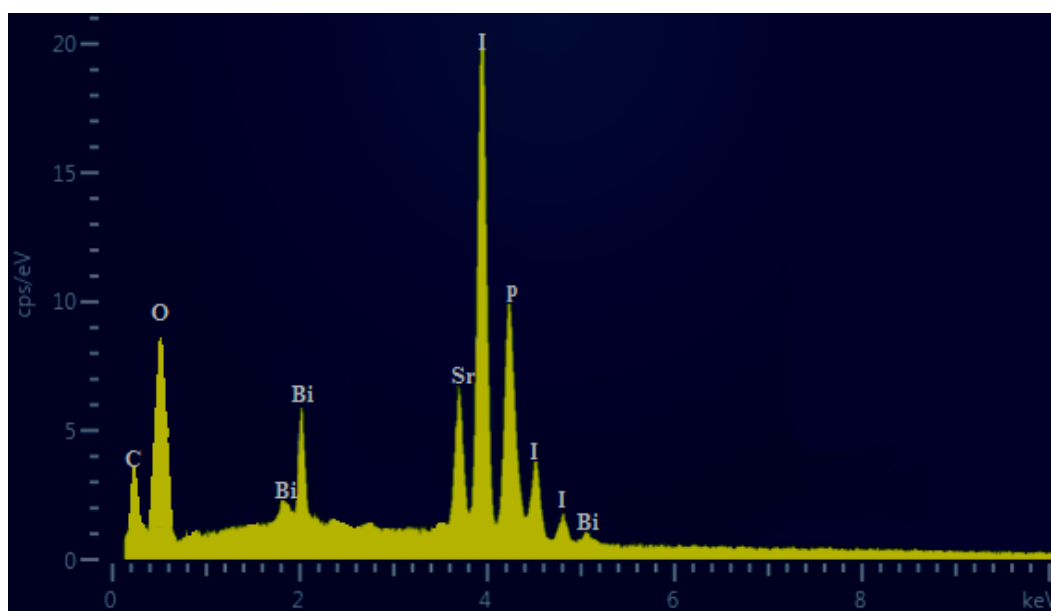


Figure 5: EDX pattern of BiOI/SrHA

5. Impact of Some Parameters on Dyes Degradation

5.1. BiOI/SrHA dosage

Figure 7 display the impact of BiOI/SrHA concentration on photocatalytic dyes decay. In the absence of BiOI/SrHA, photodegradation for BF and CV is (5 and 3.5)%, correspondingly. believe that ultraviolet light alone is

insufficient to oxidize dyes included in colorful wastewater samples; photocatalysts must be used to activate the UV. It is when the use of BiOI/SrHA is as a photocatalyst with UV yielded a significant improvement of dyes decay on the contrary when using UV alone to decay dyes⁽²⁴⁾. The nanoparticles BiOI on SrHA as support is an experimentally efficient

photocatalyst that uses light energy to form the e-/h+ pair on its surface. Where this pair works e-/h+ on decomposing the dyes through the formation of active oxygen species superoxide radical anions ($O_2^{\bullet-}$) and hydroxyl radicals (HO^{\bullet}) Which is the main factors in the pollutants decay. The kinetics of photocatalytic dye degradation by the photocatalyst BiOI/SrHA were investigated at zero-order (eq. 1), first-order (eq. 2), and second-order (eq. 3).

$$C_0 - C = k_0 t \text{ -----}$$

(2)

$$\ln (C_0/C) = k_1 t \text{ -----}$$

(3)

$$1/C = k_2 t + 1/C_0 \text{ -----}$$

(4)

where C_0 and C are the initial dye absorbance and dye absorbance at time t , respectively. The rate constants k_0 , k_1 , and k_2 denote the zero-order, first-order, and second-order, correspondingly. To illustrate the applicability of zero-order, first-order, and second-order kinetics models for photocatalytic dye degradation by the nanoparticle of BiOI/SrHA at various catalyst dosages, linear plots of $C_0 - C$ versus different irradiation time (t) Figure 8, $\ln (C_0/C)$ versus different irradiation time (t) Figure 9, and $1/A$ versus different irradiation time (t) Figure 10 are plot. The correlation coefficient values k_0 , k_1 , and k_2 , R^2 are displayed in (Table 1,2). The results indicated that the kinetics of photocatalytic dye degradation via BiOI/SrHA followed a first-order kinetic at varying catalyst concentrations.

The following experiments were performed at pH 7 and temperature 30 ± 5 °C.

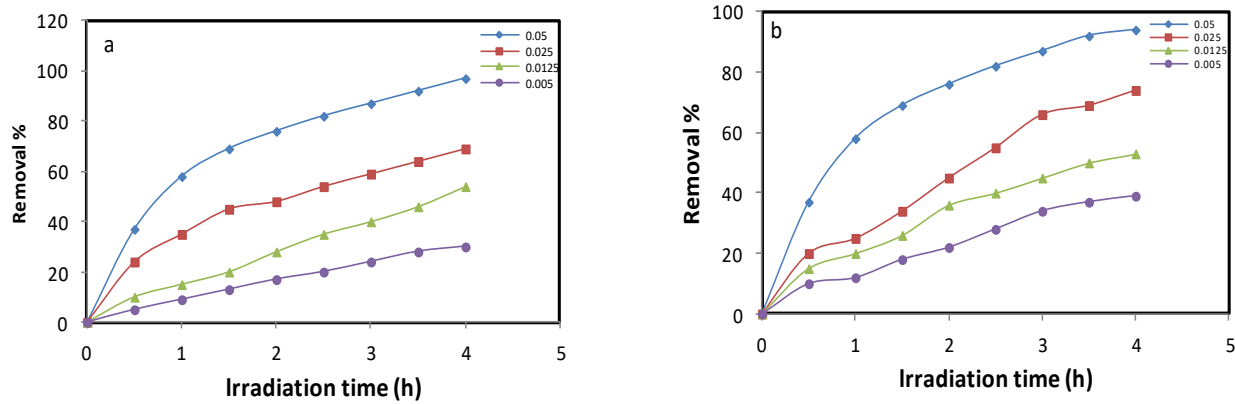


Figure 6: The effect of BiOI/SrHA dose on the degradation of dyes in the presence of UV/BiOI/SrHA BF(a) and CV(b)

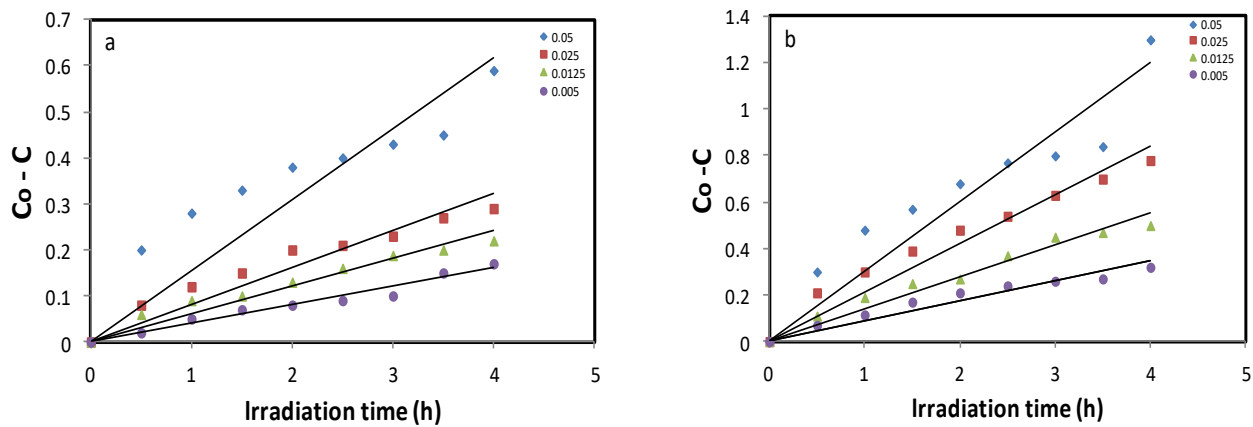


Figure 7: shows the zero-order kinetics of photocatalytic dye degradation using BiOI/SrHA at varied catalyst concentrations BF(a) and CV (b)

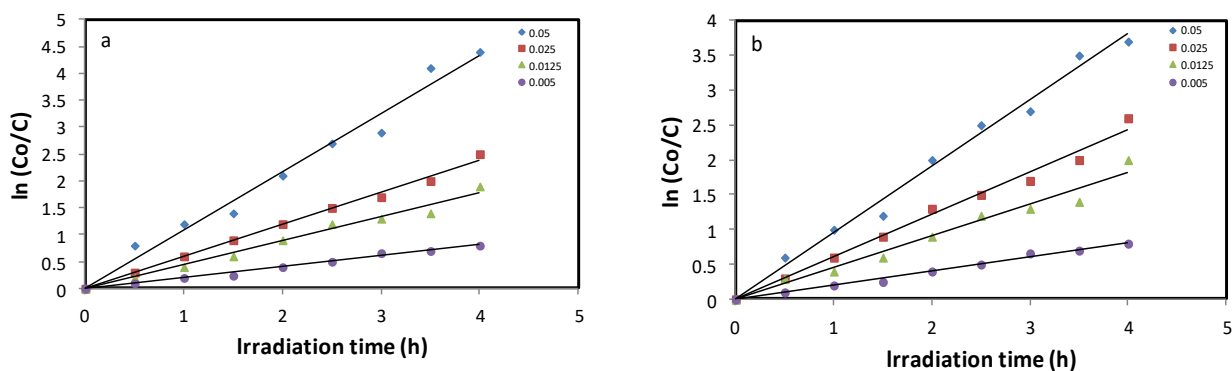


Figure 8: shows the first-order kinetics of photocatalytic dye degradation using BiOI/SrHA at varied catalyst concentrations BF(a) and CV (b)

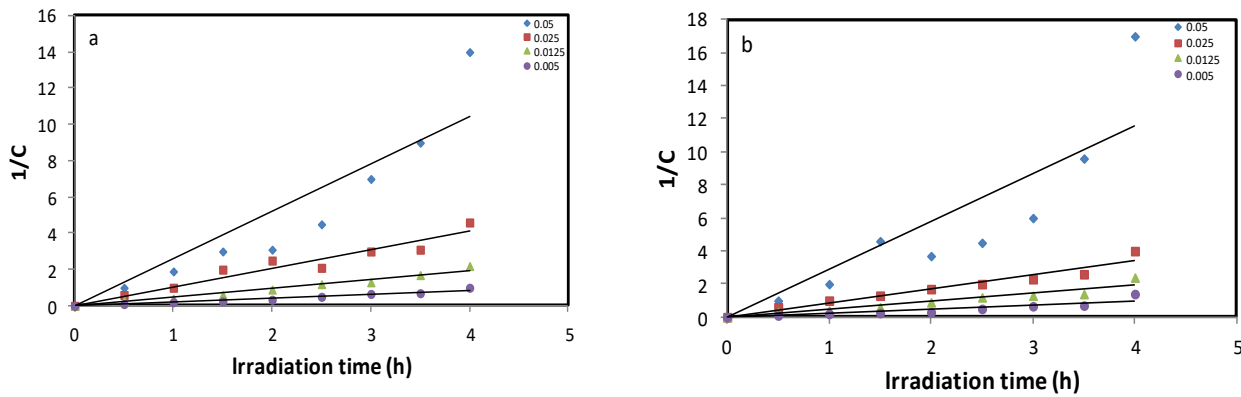


Figure 9: shows the second-order kinetics of photocatalytic dye degradation using BiOI/SrHA at varied catalyst concentrations BF(a) and CV (b)

Table 1: The kinetics constants of photocatalytic Basic Fuchsin dye degradation by BiOI/SrHA at various catalyst dosages

BiOI/SrHAp (g)	zero-order kinetic		first-order kinetic		second-order kinetic	
	K ₀	R ²	K ₁	R ²	K ₂	R ²
BF						
0.05	2.611	0.7538	0.1795	0.9797	0.2145	0.853
0.025	0.1589	0.9021	0.146	0.9946	0.0274	0.93
0.0125	0.0265	0.9359	0.0693	0.9713	0.0754	0.9697
0.005	0.0749	0.9643	0.0678	0.9908	0.3428	0.9553

Table 2: The kinetics constants of photocatalytic Crystal Violet dye degradation by BiOI/SrHA at various catalyst dosages

BiOI/SrHAp (g)	zero-order kinetic		first-order kinetic		second-order kinetic	
	K ₀	R ²	K ₁	R ²	K ₂	R ²
CV						
0.05	0.6322	0.8696	0.6899	0.9883	2.6954	0.7705
0.025	0.0698	0.9332	0.6874	0.988	0.1252	0.9442
0.0125	0.0534	0.9535	0.2199	0.9713	0.2114	0.9161
0.005	0.0419	0.9218	0.1025	0.9908	0.2773	0.8139

5.2. Initial dye concentration

Figure 10 displays the impact of initial dye concentration on photocatalytic dye decay at various time intervals. The results offer that dye degradation decreases through initial dye concentration increasing. With the increase in the dye concentration, the potential reason is the intervention from intermediates composed upon the decay of the parental dye molecules. Such repression would be more obvious in the presence of a high level of degradation intermediates composed upon an increased initial dye concentration⁽²⁵⁾. To insert the application of the zero-order, first-order, and second-order kinetics types for photocatalytic

dye degradation by the nanoparticles at various initial dye concentrations, linear plots of $C_0 - C$ versus irradiation time (t) for zero-order model Figure 11, $\ln (C_0/C)$ versus irradiation time (t) for first-order order model Figure 12, and $1/C$ against irradiation time (t) for second-order types Figure 13 are plotted. The values of k_0 , k_1 , and k_2 , R^2 (correlation coefficient values) are shown in Table 3 and 4. The outcome showed that the kinetics of photocatalytic dye degeneration by BiOI/SrHA at various initial dye concentrations followed the first-order kinetic type.

The following experiments were performed at pH 7 and temperature 30 ± 5 °C.

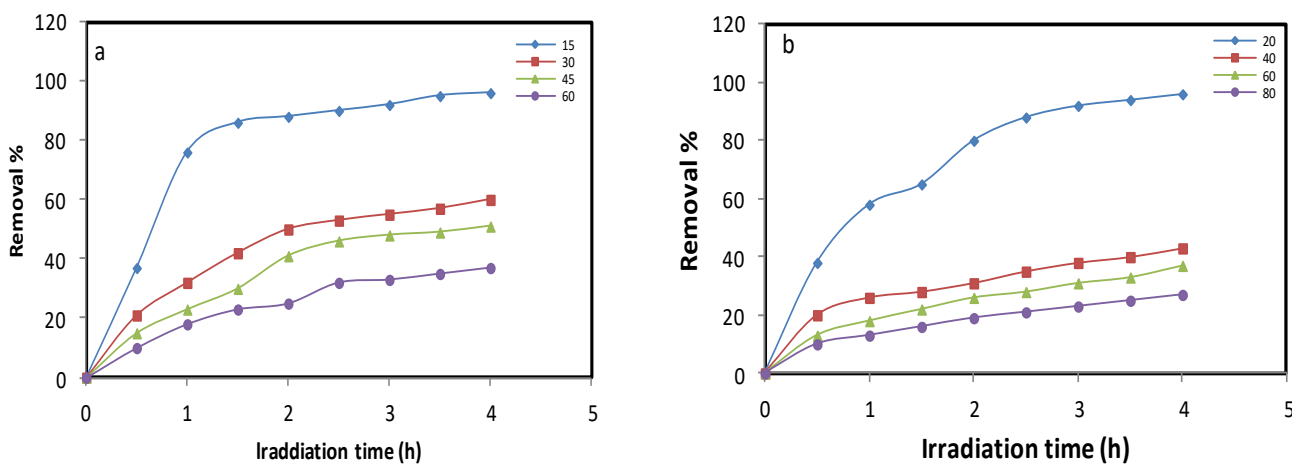


Figure 10: dye concentration effect on the degradation of dyes using UV/BiOBr/ SrHA (a) BF, and (b) CV

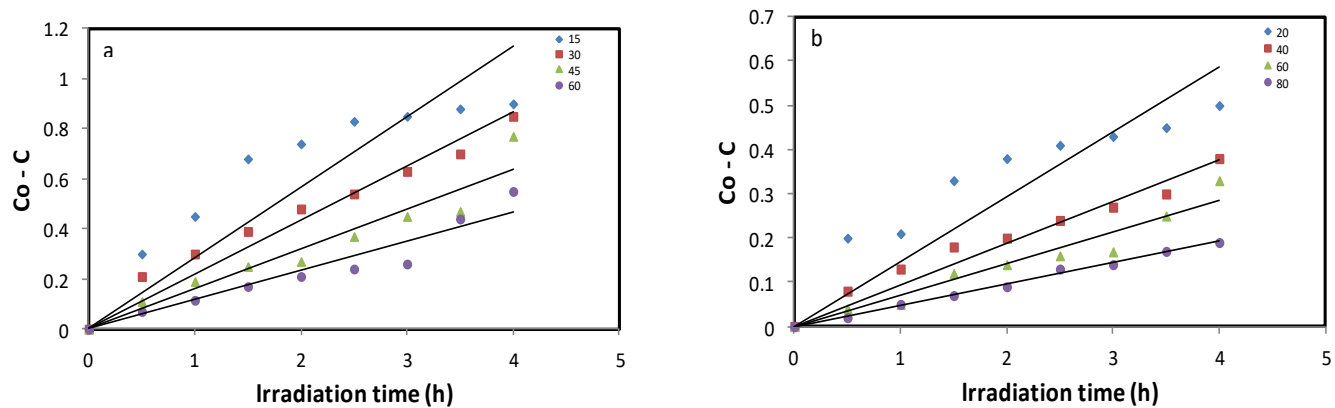


Figure 11: The zero-order kinetic of photocatalytic dye degradation by BiOBr/ SrHA different dye concentrations (a) BF, and (b) CV

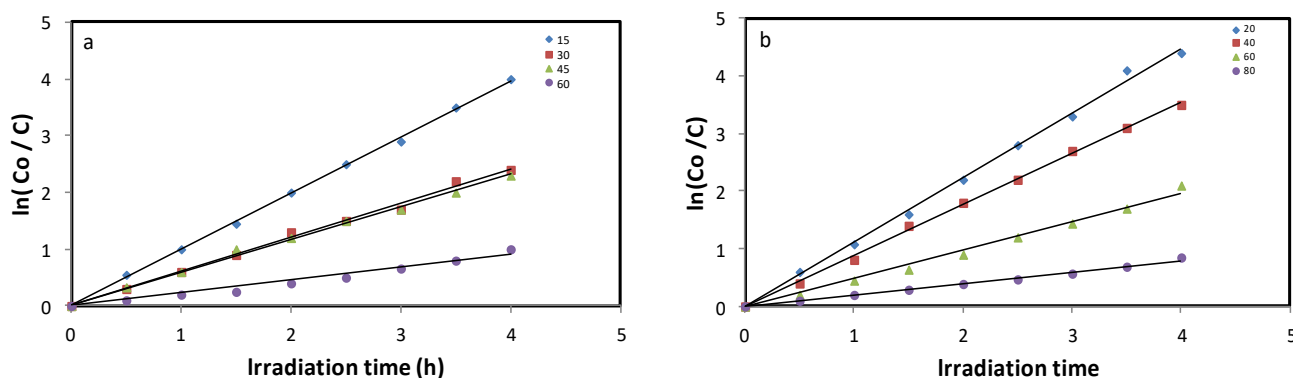


Figure 12: The first-order kinetic of photocatalytic dye degradation by BiOBr/ SrHA different dye concentrations (a) BF, and (b) CV

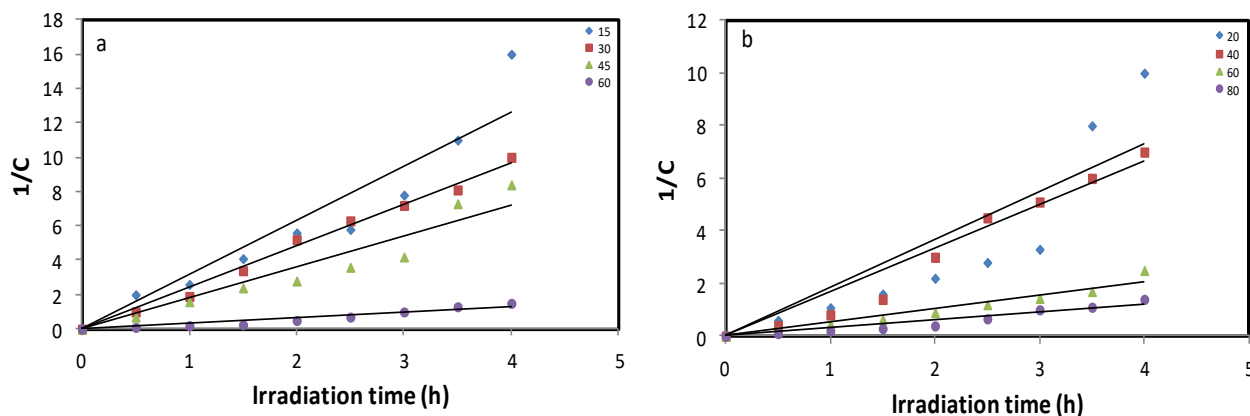


Figure 13: The second-order kinetic of photocatalytic dye degradation by BiOBr/ SrHA different dye concentrations (a) BF, and (b) CV

Table 3: The kinetics constants of photocatalytic dye degradation by BiOI/SrHA at various Basic Fuchsin dye concentrations

BiOI/SrHAp (g)	zero-order kinetic		first-order kinetic		second-order kinetic	
	K ₀	R ²	K ₁	R ²	K ₂	R ²
BF						
15	0.2842	0.6584	0.3168	0.9971	8.7496	0.7155
30	0.4231	0.9659	0.3012	0.9884	0.4984	0.9509
45	0.2123	0.9404	0.8602	0.9869	0.1429	0.9693
60	0.0278	0.9316	0.4649	0.9945	0.1584	0.9431

Table 4: The kinetics constants of photocatalytic dye degradation by BiOI/SrHA at various Crystal Violet dye concentrations

BiOI/SrHAp (g)	zero-order kinetic		first-order kinetic		second-order kinetic	
	K ₀	R ²	K ₁	R ²	K ₂	R ²
CV						
20	0.2551	0.871	0.3816	0.9847	2.4523	0.8553
40	0.3254	0.9209	0.2943	0.9611	0.1587	0.7642
60	0.3719	0.8367	0.2442	0.9944	0.3324	0.922
80	0.3022	0.8344	0.1378	0.9838	0.0558	0.8857

6. Conclusions

The results show that BiOI-supported SrHA is an efficient adsorbent for the removal of Basic Fuchsin (BF) and Crystal Violet (CV) dyes from aqueous solutions, and because of its higher capacity, it can be used in wastewater treatment. The increased photocatalytic activities of BiOI/SrHA could be referred to as the formation of the heterojunction between BiOI and SrHA, which helpfully restrain the recombination of electron-hole pairs. Both the photocatalytic process and the photosensitized process would work concurrently, $\cdot\text{OH}$ and $\text{O}_2^{\cdot-}$ are two main active types in the photocatalytic process. In the photocatalytic process, N-de-methylation and conjugated structure of CV and BF dyes occur during the decomposition process with BiOI/SrHA starting the catalyst. Therefore, it can

be concluded that BiOI/SrHA provides a heterogeneous surface for the adsorption of dyes. The outcome display that the modified adsorbent is a strong UV photocatalyst.

7. REFERENCES

- [1] Rakness, Kerwin L., et al. "Wastewater disinfection with ozone-process control and operating results." *Ozone: science & engineering* 15.6 (1993): 497-513.
- [2] Raizada, Pankaj, et al. "Fabrication of Ag₃VO₄ decorated phosphorus and sulphur co-doped graphitic carbon nitride as a high-dispersed photocatalyst for phenol mineralization and E. coli disinfection." *Separation and purification technology* 212 (2019): 887-900.

3. [3] Pare, Brijesh, Pardeep Singh, and S. B. Jonnalagadda. "Visible light-driven photocatalytic degradation and mineralization of neutral red dye in a slurry photoreactor." (2010).
4. [4] B. Pare, P. Singh, S.B Jonnalagadda, Artificial light assisted photocatalytic degradation of flossamine fast yellow dye in ZnO suspension in a slurry batch reactor, Indian J. Chem., Sect A 48 A (2009) 1364-1369
5. [5] Zhang, Lisha, et al. "Sonochemical synthesis of nanocrystallite Bi₂O₃ as a visible-light-driven photocatalyst." Applied Catalysis A: General 308 (2006): 105-110.
6. [6] Asahi, R. Y. O. J. I., et al. "Visible-light photocatalysis in nitrogen-doped titanium oxides." science 293.5528 (2001): 269-271.
7. [7] Khan, Shahed UM, Mofareh Al-Shahry, and William B. Ingler. "Efficient photochemical water splitting by a chemically modified n-TiO₂." science 297.5590 (2002): 2243-2245.
8. [8] Al-Rubaie, Ali Z., Inas K. Mohammed, and Zaki N. Kadhim. "Synthesis and Characterization of New Organotellurium (IV) Compounds Containing Carbodithioate Ligands." IOP Conference Series: Materials Science and Engineering. Vol. 928. No. 5. IOP Publishing, 2020.
9. [9] Singh, Pardeep, et al. "Preparation of BSA-ZnWO₄ nanocomposites with enhanced adsorptional photocatalytic activity for methylene blue degradation." International Journal of Photoenergy 2013 (2013).
10. [10] Li, Shijie, et al. "A novel heterostructure of BiOI nanosheets anchored onto MWCNTs with excellent visible-light photocatalytic activity." Nanomaterials 7.1 (2017): 22.
11. [11] Xiang, Yuhui, et al. "Chemical etching preparation of the Bi₂WO₆/BiOI p-n heterojunction with enhanced photocatalytic antifouling activity under visible light irradiation." Chemical Engineering Journal 288 (2016): 264-275.
12. [12] Chen, Lang, et al. "Room-Temperature Synthesis of Flower-Like BiOX (X = Cl, Br, I) Hierarchical Structures and Their Visible-Light Photocatalytic Activity." Inorganic chemistry 52.19 (2013): 11118-11125.
13. [13] Radhi, Ibtighaa Kadhim, Mouayed Abdulaali Hussein, and Zaki Naser Kadhim. "Investigation of nigrosine, alizarin, indigo and acid fuchsin removal by modification of CaO derived from eggshell with AgI: Adsorption, kinetic and photocatalytic studies." European Journal of Chemistry 10.1 (2019): 64-71.
14. [14] Jiang, Zaiyong, et al. "Enhancing visible light photocatalytic degradation performance and bactericidal activity of BiOI via ultrathin-layer structure." Applied Catalysis B: Environmental 211 (2017): 252-257.
15. [15] Luan, Jingfei, et al. "Growth, structural and photophysical properties of i₂GaTaO₇." Journal of crystal growth 273.1-2 (2004): 241-247.
16. [16] Di, Jun, et al. "Bidirectional acceleration of carrier separation spatially via N-CQDs/atomically-thin BiOI nanosheets nanojunctions for manipulating active species in a photocatalytic process." Journal of Materials Chemistry A 4.14 (2016): 5051-5061.
17. [17] Jiang, Zaiyong, et al. "Enhancing visible light photocatalytic degradation performance and bactericidal activity of BiOI via ultrathin-layer structure." Applied Catalysis B: Environmental 211 (2017): 252-257.
18. [18] Di, Jun, et al. "Reactable ionic liquid-assisted rapid synthesis of BiOI hollow microspheres at room temperature with enhanced photocatalytic activity." Journal

- of Materials Chemistry A 2.38 (2014): 15864-15874.
20. [19] Hasan, Jaafar, et al. "Efficient visible-light-driven photocatalysis of flower-like composites of AgI nanoparticle dotting BiOI nanosheet." *Journal of Solid State Chemistry* 297 (2021): 122044.
21. [20] Ye, Liqun, et al. "Synthesis of highly symmetrical BiOI single-crystal nanosheets and their {001} facet-dependent photoactivity." *Journal of Materials Chemistry* 21.33 (2011): 12479-12484.
22. [21] Xiao, Xiufeng, et al. "Structural characterization of zinc-substituted hydroxyapatite prepared by hydrothermal method." *Journal of materials science: Materials in medicine* 19.2 (2008): 797-803.
23. [22] Radhi, Ibtighaa Kadhim, Mouayed Abdulaali Hussein, and Zaki Naser Kadhim. "Investigation of nigrosine, alizarin, indigo and acid fuchsin removal by modification of CaO derived from eggshell with AgI: Adsorption, kinetic and photocatalytic studies." *European Journal of Chemistry* 10.1 (2019): 64-71.
24. [23] AS Alassadi, Erfan, Zaki N Kadhim, and Mazin N Mousa. "The In Vitro Release Study Of Ceftazidime drug From Synthesized Strontium Flourapatite And Strontium Hydroxyapatite Coated Particles." *karbala journal of pharmaceutical sciences* 8.13 (2017): 137-151.
25. [24] Simon, V., et al. "Microscopic analysis of sintered titanium-hydroxyapatite implant materials." *Journal of Optoelectronics and Advanced Materials* 7.6 (2005): 2823.
26. [25] Kumar, Ankit, and G. Pandey. "A review on the factors affecting the photocatalytic degradation of hazardous materials." *Mater. Sci. Eng. Int. J* 1.3 (2017): 1-10.